BILINGUAL PUBLISHING CO.
Pioneer of Global Academics Since 1984

Journal of Construction Research
https://ojs.bilpublishing.com/index.php/jcr-b

ARTICLE

Effects of Lizardite Addition on Technological Properties of Forsterite-monticellite Rich Ceramics Prepared from Natural Magnesite and Dolomite

Ahmed Manni[1] Achraf Harrati[1] Abdelilah El Haddar[2] Abdelwahed Chari[3] Ali Sdiri[4] Fahd Oudrhiri Hassani[5] Abdeslam El Bouari[1] Iz-Eddine El Amrani El Hassani[6] Chaouki Sadik[1*]

1. Laboratory of Physical Chemistry of Applied Materials (LPCMA), Department of Chemistry, Faculty of Sciences Ben Msik, Hassan II University of Casablanca, Morocco
2. Laboratory of Applied Geosciences, Faculty of Sciences, University of Mohammed 1, Oujda, Morocco
3. Materials Sciences, Energy and Nano-engineering Department, Mohammed VI Polytechnic University, Ben Guerir, Morocco
4. Department of Georessources and Environment, National Engineering School, University of Sfax, P. Box 3052, Sfax, Tunisia
5. LMPEQ, University of Cadi Ayyad, ENSA of SAFI, Morocco
6. Geomaterials and Geo environment Team/Geo-Biodiversity and Natural Patrimony Laboratory, (GEOBIO)/Geophysics, Natural Patrimony and Green Chemistry Research Centre (GEOPAC), Scientific Institut, Mohammed V University of Rabat, Morocco

ARTICLE INFO

Article history
Received: 11 December 2020
Accepted: 29 December 2020
Published Online: 31 January 2021

Keywords:
Forsterite
Monticellite
Lizardite
Basic ceramics
Temperature

ABSTRACT

Lizardite rich peridotite has never been used to prepare ceramic specimens, especially in Morocco. For this raison, potential use of naturally abundant lizarditic material from the Rif domain, as a supply for ceramic industry, has been evaluated. The effects of lizardite addition to magnesite and dolomite mixtures on the thermomechanical properties of the calcined ceramics were also detailed. To achieve this target, natural lizardite, magnesite and dolomite samples were collected in ultrabasic Beni Bousra massif. Those raw samples were used for the synthesis of a forsterite-monticellite rich ceramics. Both raw and sintered samples were characterized by x-ray diffraction, scanning electron microscope and fourier transform infrared. The obtained results showed that both magnesite and dolomite were mainly composed of MgCO3 and CaCO3. In contrast, lizardite sample showed high amounts of SiO2, MgO and Fe2O3. An increased amount of lizardite in the initial mixtures enhanced mechanical and dimensional properties of the prepared ceramic specimens, and subsequently, the production of ceramics with the required technological properties. Thus, the preparation of Moroccan lizardite-based ceramics is technically feasible, economically justifiable and socially desirable due to the contribution to the economic growth of the raw materials sector, especially ceramic industry.

**Corresponding Author:*
Chaouki Sadik,
Laboratory of Physical Chemistry of Applied Materials (LPCMA), Department of Chemistry, Faculty of Sciences Ben Msik, Hassan II University of Casablanca, Morocco;
E-mail: schawki37@gmail.com

 DOI: https://doi.org/10.30564/jcr.v2i1.2684

1. Introduction

In the face of ever-increasing developments and numerous innovations in the ceramic industry, including refractories, the field of mass-market ceramics, in which the wide variety of pyroprotection applications in industry requires a wide diversity of ceramic material supplies. In fact, many of these materials have been developed specifically to meet the operating conditions of a particular process. The characteristic properties of each ceramic class depend on both the raw material used and the manufacturing methods of the ceramic products [1-8]. The type of ceramic to be used is often dictated by the conditions prevailing in the area of application. In the high temperature range, some refractory metal alloys can be used, but their use remains limited below 1000°C. Beyond that, only refractory materials are thermally and mechanically resistant [9].

Today, silica-alumina ceramics are widely used for lining furnaces (refractories), tiles, bricks, ladles, glass tank controllers and secondary refining vessels in ferrous and non-ferrous metallurgy, due to their high degree of refractoriness, high thermal shock resistance and excellent slag resistance [10-11]. At the same time, basic refractories can also be used in various fields as excellent robust material, resistant to heat and electricity, as well as good heat conductor [12]. To date, several research projects have been devoted to the recovery of materials in the field of ceramics, in particular the development and characterization of basic refractory ceramics due to their high refractory quality and their resistance to erosion and corrosion of metals and oxides [13-23].

Due to the growing concern about the economy and the recovery of the basic ceramic industry in Morocco, it is becoming imperative and crucial to look for new raw materials containing magnesium. However, the main focus of discussion only to use three essential minerals forming the rocks: Magnesite, dolomite and lizardite situated in the Rif of Morocco, and which has other secondary materials: perlite, halloysite, diatomite, bentonite and red clays [24-25].

However, detailed studies on Moroccan lizardite-based ceramics are missing. Thus, the present study has been carried out to evaluate the potential use of abundant raw materials from Morocco (i.e., lizardite, magnesite and dolomite) for the preparation of a forsterite-monticellite rich ceramics with the required technical specifications (i.e., high mechanical performances).

2. Materials and Methods

2.1 Collection and Preparation of the Raw Samples

The ultrabasic Beni Bousra massif in the Inner Rif (Morocco) is one of the most important peridotite massifs in the western Mediterranean area. It contains useful geomaterials that can be valorized for ceramic industry. For the purpose of the current study, a lizarditeic clay rich peridotite, dolomite and magnesite samples were collected in the Beni Bousra massif (internal Rif, Morocco) belonging to the Tafidest area to the south-western edge of the Tetouan city (about 103 km SW) (Figure 1). Peridotite from Beni Bousra is an ultrabasic rock which outcrops on the surface in the internal domain of the Rif Alpine range. Peridotite is a plutonic rock of very deep origin (upper mantle) and whose rise and establishment in the crust occur in the context of the retreat of the Alpine subduction towards the South and West during the Oligo-Miocene. The peridotite shows towards the center of the massif a fresh aspect where the rock is bottle-green in color and composed of rounded grains of green olivine distributed over a black background composed of ferro-magnesian minerals (pyroxene, amphibole and biotite) (Figure 2.A). Towards the edge of the massif and along the fractures, the rock becomes weathered and friable (Figure 2.B). Microscopic observation of peridotite shows that olivines and pyroxenes are often cut into fragments (brecciated) and altered into serpentine (antigorite and lizardite). In friable peridotite, there are no longer any primary minerals (olivine and pyroxene); most of the rock is serpentinized.

Magnesite and dolomite were collected from the coordinates N35°13'11.5" W004° 43'49.1" while lizardite clay deposits come from N35° 16'42,9" W004° 51'41.82"). Prior to the different analyses, the collected natural raw materials were hand crushed using a stainless steel mortar and pestle, sieved and a grain size of less than 500 µm was reclaimed and stored in plastic bottles. Further grinding was undertaken when necessary to prepare subsamples for subsequent physico-chemical characterization and ceramic specimen preparation.

DOI: https://doi.org/10.30564/jcr.v2i1.2684

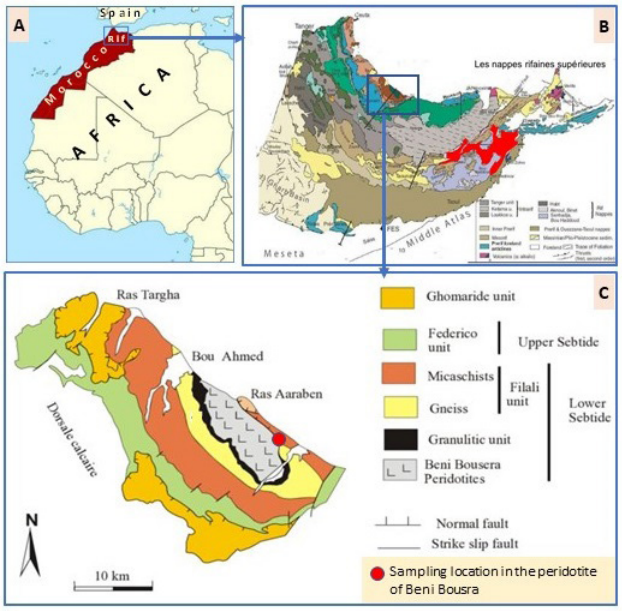

Figure 1. A: Situation of Morocco on the scale of Africa- B: Geological map of the Rif - C: Structural diagram of the environment of the ultrabasic peridotite massif of Beni Bousra with sampling location [26]

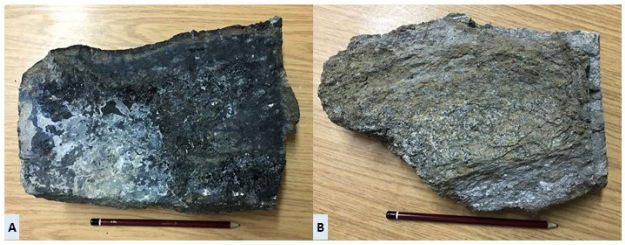

Figure 2. Macroscopic appearance of Beni Bousra's peridotite

2.2 Chemical and Mineralogical Analyses

Chemical compositions of the powdered and pressed samples from the ultrabasic Beni Bousera massif (Morocco) was determined by using a fluorescence spectrometer type 'SPECTRO' (AMETEC company, MOROCCO). XRD analysis was performed on using PANalytical XPert Pro diffractometer equipped with Cu kα radiation (Kα1 = 1.5406 Å, 45 kV and 40 mA). Randomly oriented powder was prepared by sieving 1g of the desired sample (i.e., lizardite, dolomite and magnesite) to 250µm, placed on a sample holder and then step scanned between 2° and 70° (2θ) with 0.02° increments. The diffractogram of each sample was recorded and then computer-processed to get the peak position and its intensity. Abundance of each mineral species present in the studied samples was estimated by the application of the external standard method [27]. FT-IR spectra were obtained with a Bruker Tensor 27 FTIR spectrometer operating in the range 4000–400 cm^{-1}.

Petrographic observation has been performed on thin sections from rock fragments with an optical microscope (Olympus BX 51TF: University Mohammed V, Rabat, Morocco). The texture (shape, size and arrangement of its mineral constituents) and the optical criteria of the minerals (habitus, color, cleavage, pleochroism, relief, polarization tint) allowed a more credible identification of the ubiquitous mineral species. Thin sections of 30 µm thick slide were cut from the desired sample, polished and stick on a glass plate before observation.

2.3 Thermo-dilatometric Analysis

The thermodilatometric test were performed by using a LINSEIS Dilatometer, type: L75 (Linseis Messgeraete GmbH, Selb, Germany) by heating the green ceramic specimen from 25 to 1600 °C at the regular increment of 5 °C/min under air atmosphere. The cycle includes two plateau of 2 h (i.e., 600 and 1200 °C).

2.4 Ceramic Preparation

Technological tests concerned the less than 63 µm sized subsamples that were dried to 105 °C for 24 hours. The dry materials are introduced into jars together with a known weight of stainless-steel balls of various diameters and distilled water (i.e., 4 and 6%). Four mixtures (M1–M4) were prepared by varying lizardite percentages from 10 to 40% (Table 1). About 100 g of the desired mixture was molded in 10 x 5 x 1 cm^3 rectangular shaped mold that was, later, compressed to prepare a green ceramic specimen; cylindrical mini-brick samples were prepared using a hydraulic press (200 bars). The prepared mini-bricks were oven dried for 24 hours and heated to the desired temperatures using an electric furnace (Nabertherm GmbH, Germany) in an oxidizing atmosphere. Heating program was set to a constant heating rate of 3 °C/min with two main plateau of 30 minutes (i.e., 600 and 1100 °C). After firing, the furnace was cooled down to room temperature with a cooling rate of 5 °C/min.

Table 1. Composition of prepared mixtures (wt. %)

Mixtures	Lizardite (%)	Magnesite (%)	Dolomite (%)
M1	10	45	45
M2	20	40	40
M3	30	35	35
M4	40	30	30

2.5 Technological Tests

To find out the main physico-chemical properties of the

 DOI: https://doi.org/10.30564/jcr.v2i1.2684

prepared ceramic specimens, a set of technological tests (i.e., flexural strength, tensile strength, shrinkage) were performed accordingly. Flexural strength measurements were conducted using a 3R type: RP25 ATF. The well-known three-point flexure test was used for testing the prepared ceramic samples according to the ASTM C674-88 normative guideline [28].

Indirect tensile strength (i.e., Brazilian test) was also used to measure the tensile strength of the prepared ceramic specimen using a press apparatus type 3R (SODAP company, Morocco) [29].

Shrinkage test was done by the measurement of the average lengths recorded on mini-brick specimen dried at 110 °C and then fired to 1100 and 1400 °C. The following formula allows the calculation of the firing shrinkage:

$$\text{Shrinkage (\%)} = \frac{L110 - Lt}{L110} \times 100 \quad (1)$$

Where Lt is the length after firing and L110 the length after drying at 110 °C.

Linear thermal expansion (α_L in $°C^{-1}$) was determined by the following relationship:

$$a_L = \frac{\Delta L}{L0 \times \Delta T} \quad (2)$$

ΔL: length variation (mm)
L_0: Initial length, expressed (mm).
ΔT: Temperature difference, expressed in K.

A thermal expansion by volume (α_V) can be deduced for an isotropic material from the following relationship [30].

$$\alpha_V = 3\alpha_L \quad (3)$$

The bulk density and apparent porosity were measured according to ASTM C373-88 [31]. In a brief description, a dried test specimen (weight= D; total volume=V) was introduced in a boiling water vessel for 5 h and left to cool down for 24h to determine the saturated mass (M). Finally, the Apparent porosity, P (%), was calculated as follows:

$$P = \frac{M - D}{V} \times 100 \quad (4)$$

Bulk density, B (g/cm^3), included pores as follows:

$$B = \frac{D}{V} \quad (5)$$

Microstructural analysis of the prepared ceramics specimens was conducted by scanning electron microscope coupled with the EDS analysis, type: Hitachi TM3000.

3. Results and Discussion

3.1 Characterization of the Raw Samples

Chemical composition, by XRF (Table 2), showed that magnesite was mainly composed of MgO (42.63%). Such a carbonaceous natural sample exhibited a high loss on ignition (LOI = 52.35%) due to its $MgCO_3$ content. Dolomite showed a similar high LOI value (51.02%), but lower MgO content (20.63%) compared to magnesite. In addition, it was expected to find higher percentage of $CaCO_3$ (40.57%), as a further proof about the dolomitic nature of the collected carbonate sample (i.e., dolomite sample). SiO_2 contents in both materials were ascertained to 1.78% and 3.06% for magnesite and dolomite, respectively. Low amounts of alumina (Al_2O_3) were found in both samples. In contrast, lizardite sample showed a predominant silica content, reaching 53.48%; followed by a relatively high magnesia content (35.39%), iron oxide (6.68%) and alumina (3.15%) together with faint amounts of Na_2O (0.9%) and CaO (0.33%). Such a chemical composition perfectly corroborated with the mineralogical composition of lizardite (predominant mineral phase).

Figure 3 represents the positions of the used raw materials on the CaO-SiO_2-MgO ternary diagram. A number

Table 2. Chemical analysis by X-ray fluorescence of raw materials (wt. %)

Samples	SiO_2	Al_2O_3	Fe_2O_3	MgO	CaO	K_2O	Na_2O	P_2O_5	MnO	SO_3	TiO_2	LOI
Dolomite	3.06	1.96	0.13	20.63	22.73	0.06	0.19	0.02	0.01	0.06	0.13	51.02
Magnesite	1.78	0.89	0.09	42.63	2.03	0.03	0.13	0.01	--	--	0.06	52.35
Lizardite	53.48	3.15	6.68	35.39	0.33	0.03	0.90	--	--	--	0.04	--

DOI: https://doi.org/10.30564/jcr.v2i1.2684

of investigations dealing with one or more of the three oxides: lime, magnesia and silica, have in recent years been carried out, as a preliminary step in the study of the rocks and minerals of the earth's crust. These studies include all of the possible binary and ternary of the CaO-SiO_2-MgO systems. The phases which occur in the ternary system are: (1) Cristobalite, SiO_2, (2) Tridymite, SiO_2, (3) Pseudowollastonite, α $CaO.SiO_2$, (4) Tricalcium di-silicate, $3CaO.\ 2SiO_2$, (5) α Calcium orthosilicate, α $2CaO.\ SiO_2$, (6) Lime, CaO, (7) Periclase, MgO, (8) Forsterite, $2MgO.SiO_2$, (9) monticellite, ($CaO.MgO.SiO_2$), (10) Diopside, ($CaO.MgO.2SiO_2$) and (11) pyroxene solid solution [32].

Nevertheless, it can be noted that if the MgO and SiO_2 amount increases, new phases such as forsterite and monticellite will appear. The used carbonate raw materials (magnesite, dolomite and lizardite) decomposed into monoxide, in combination with SiO2, form new phases such as forsterite ($2MgO\ SiO_2$), monticellite ($CaO.MgO.\ SiO_2$) and diopside ($CaO.MgO.2SiO_2$) [33]. Olivine could also be observed as an intermediate phase before forsterite formation occurs, depending on the relative proportions of the three components (SiO_2, MgO, CaO) and the firing temperature.

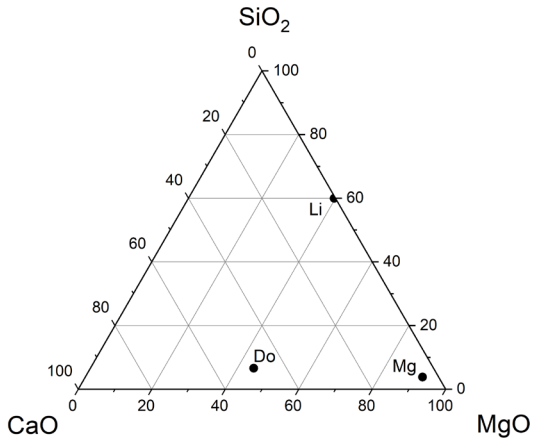

Figure 3. Classification of the studied raw materials based on CaO-SiO_2-MgO ternary diagram (Li: Lizardite, Do: Dolomite and Mg: Magnesite)

As shown in Figure 4, lizardite sample contains lizardite and antigorite phases. Dolomite sample is composed mainly of dolomite mineral as major element as well as periclase, quartz, chlorite and goethite as minor components. The magnesite sample is composed essentially of magnesite minerals. Reflections of periclase, chlorite were also observed with low intensity peaks [34]. Those observations were confirmed by the semi-quantified estimations (Table 3).

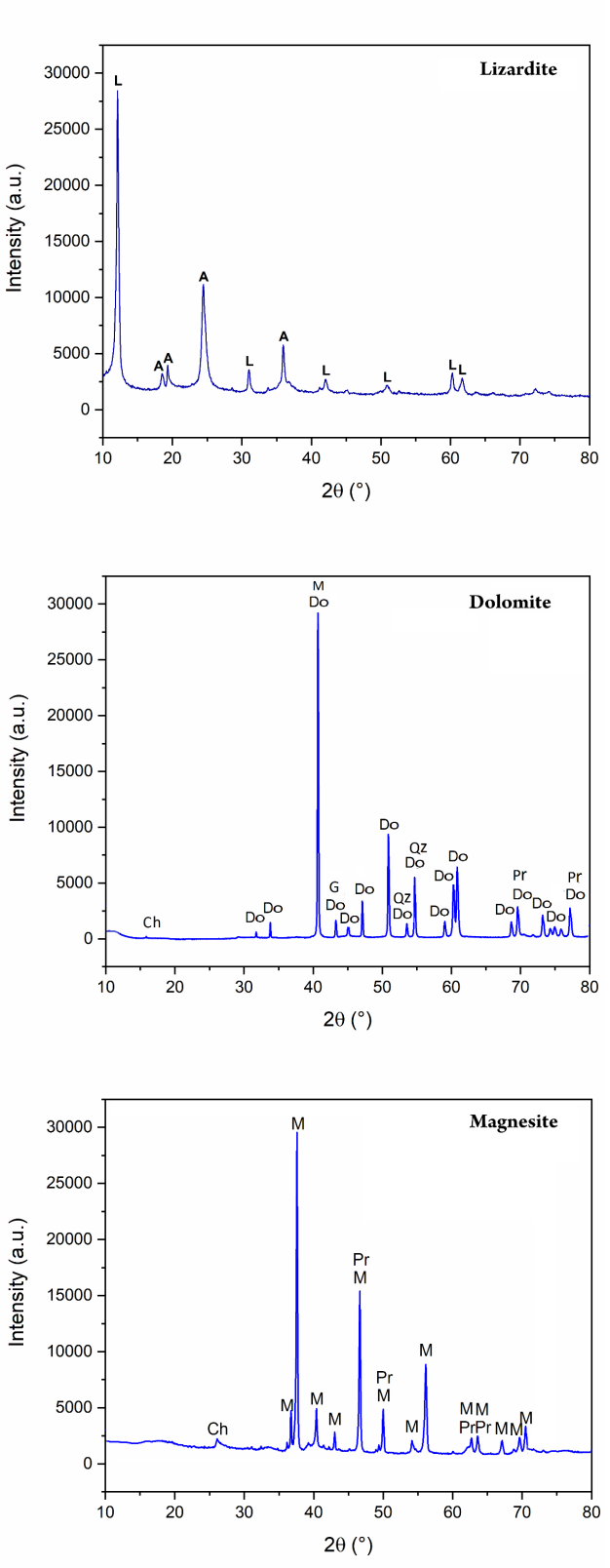

Figure 4. X-ray diffractograms of the studied Lizardite (a), Dolomite (b) and Magnesite (c). L: Lizardite, A: Antigorite, Qz: Quartz, Do: Dolomite, M: Magnesite, Pr: Periclase, G: Goethite, Ch: Chlorite)

 DOI: https://doi.org/10.30564/jcr.v2i1.2684

Table 3. Semi-quantitative analysis of the studied raw materials based on XRD diffractograms (%)

	Lizard-ite	Antigo-rite	Quartz	Dolo-mite	Magne-site	Goethite	Peri-clase	Total
Lizard-ite	67.12	30.69	1.69	-	-	-	-	99.5
Dolo-mite	-	-	3.9	74.2	-	0.8	20	98.9
Magne-site	-	-	-	2.5	80.5	-	16.8	99.8

IR spectra given in Figure 5, showed the main characteristic bands of lizardite, dolomite and magnesite samples. Lizardite IR spectra showed the presence of a small amount of organic matter due their characteristic bands at 2846 and 2921 cm^{-1} [35]. A broad band at about 3422 cm^{-1} showed the presence of sepiolite (Si-O-Mg vibration) [36]. Iron hydroxide vibrated between 571 and 633 cm^{-1}; Si-O band near 1038 cm^{-1}. The bands attributed to deformation of C-O groups (i.e., carbonates) can be observed at 850 and 1458 cm^{-1} [33]. Concerning dolomite sample, wide bands observed near 1695, 3611, 3642 and 3672 cm^{-1} were attributed to the vibration mode of O-H groups. Moreover, the presence of dolomite has been confirmed by three characteristic bands near 725, 1743 and 2536 cm^{-1} in dolomite and magnesite materials. Another band at 1506 cm^{-1} in the magnesite spectrum suggested C-O bending [37]. At a lower frequency range, bands detected at 538, 598, 640 and 990 cm^{-1} are assigned to the Si-O-Mg vibrations. Two bands at 883 and 1450 cm^{-1} are also observed, as they correspond to the bands of the Mg-O bonds [38-39].

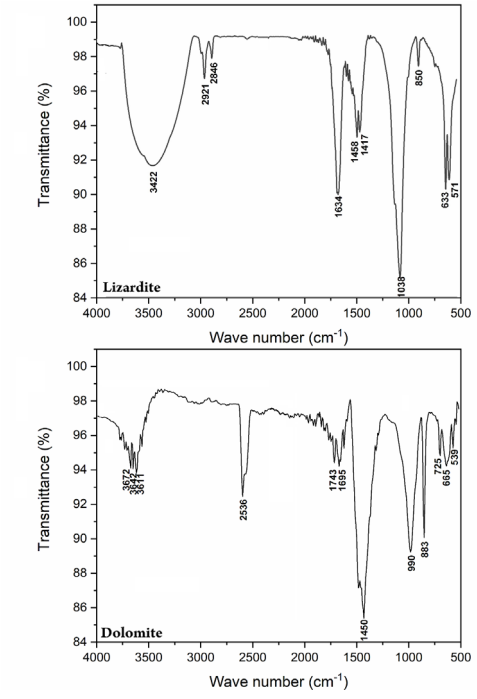

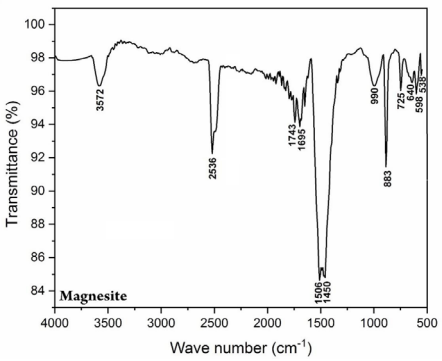

Figure 5. FTIR spectra of the studied lizardite (a), dolomite (b) and magnesite samples (c)

Dilatometric analysis of magnesite and dolomite, after heat treatment up to 1200°C, showed a clear difference in their shrinkage behaviors (Figure 6). Dilatometric curves of magnesite and dolomite showed similar trends with a first shrinkage, occurred between 600°C and 825°C, due to the decomposition of carbonates. Then, the transformation to periclase started from 850°C upwards. A total drop around 1200°C indicated a structural rearrangement of periclase. It can be seen that the shrinkage was far larger than the expansion rate (ΔL/L0 was -14% and -15% for dolomite and magnesite, respectively). Similar behavior was observed for lizardite sample, but to a somewhat lower extent (-13%).

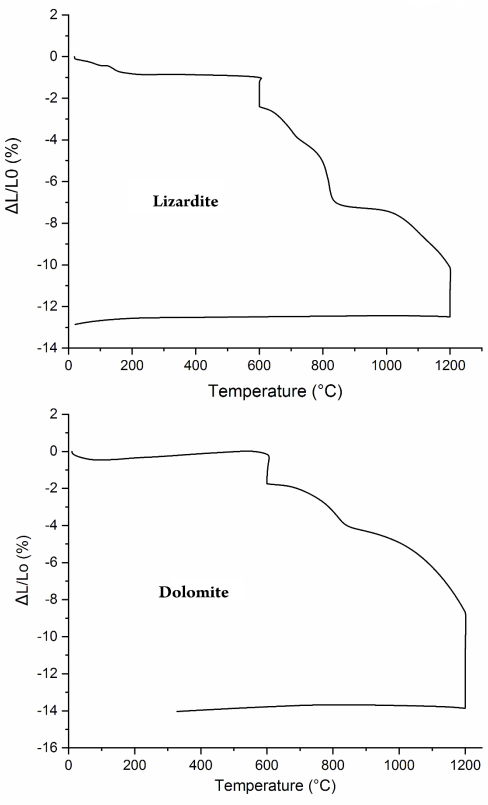

DOI: https://doi.org/10.30564/jcr.v2i1.2684

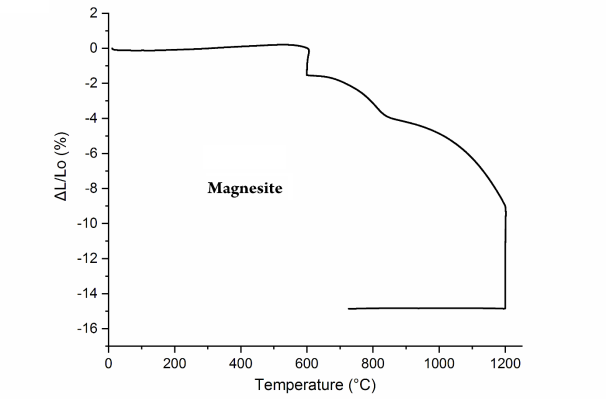

Figure 6. Thermodilatometric curves of the studied natural samples

Microscopic observations of the prepared thin sections indicated dominant dolomite minerals (Figure 7.a); a heterogeneous texture composed of finely graded masses of dolomite cut by veins of secondary alteration products. Micrographs A and B taken respectively in natural light (LN) and polarized light (LP) show the finely graded mass of dolomite recognizable by its high polarization (of the 3rd and 4th order on the Newton chromatic scale). High magnification revealed that the late veinlets crossing the dolomite mass were mainly composed of chlorite, periclase, quartz and some opaque grains (i.e., iron oxides: goethite). Magnesite sample showed a granoblastic texture with millimeter-sized joined grains of magnesite minerals (Figure 7.b). Magnesite is recognizable on both micrographs A and B by its almost orthogonal double cleavage and its high polarization shades with pink and green iridescence. At high magnifications, the magnesite grains showed small muscovite/chlorite flakes, calcite, periclase and rare opaque grains of hematite or goethite as accessory minerals. It should be noted that the mineralogical compositions of the both samples (Dolomite and Magnesite), revealed by optical microscope observations, corroborate XRD data.

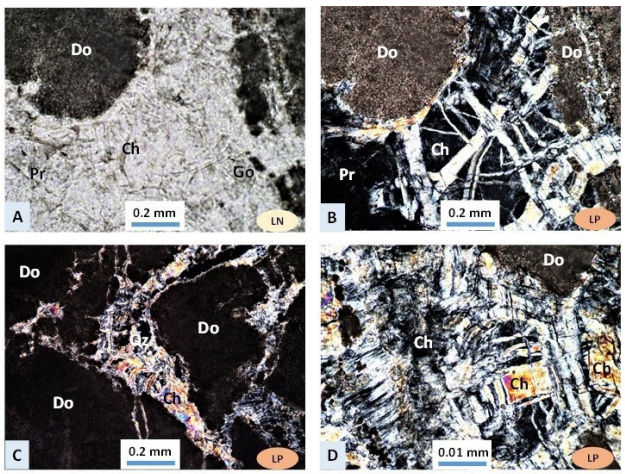

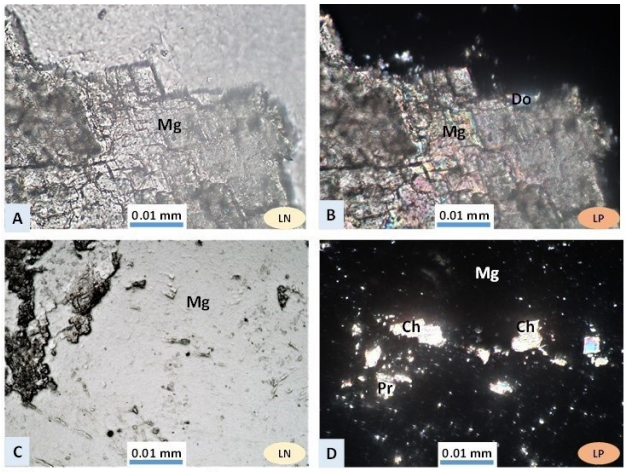

Figure 7. Microscopic observation of thin section from the dolomite (a) and magnesite samples (b) (LN: natural light, LP: Polarized light - Do: dolomite; Mg: Magnesite; Ch: Chlorite; Go: Goethite; Pr: Periclase; Qz: Quartz)

3.2 Characterization of Ceramics

Mineralogical analysis, by XRD, of the prepared ceramic samples is shown Figure 8. It is obvious that the dolomite and magnesite decomposed to free magnesia, and transformed to forsterite in the range of 780–1400 °C [40]. XRD pattern of M1 sample (10% of lizardite) showed a predominant periclase with traces of montecellite and calcium-alumino-ferrite phase. Porous oxides are formed during the decomposition of dolomite with a variation in molar volumes ranging from 62.94 cm^3 mol^{-1} for $CaMg(CO_3)_2$ to 16.92 cm^3 mol^{-1} for CaO and 11.26 cm^3 mol^{-1} for MgO. After calcination, the resulting oxides have lower molar volumes, larger surfaces and greater porosity than carbonates. The thermal decomposition of dolomite and magnesite are similar [41-43]:

$$CaMg(CO_3)_2 <===> CaCO_3 + MgO + CO_2 \quad (6)$$

$$CaCO_3 <===> CaO + CO_2 \quad (7)$$

An endothermic reaction corresponded to magnesite decomposition occurs from 800 °C. Its calcination reaction can written as follow:

$$MgCO_3 <===> MgO + CO_2 \quad (8)$$

XRD diffractograms of the prepared samples (i.e., M2, M3 and M4) are mainly composed of forsterite and monticellite, with a minor periclase, cristobalite and olivine. The intensity peak of forsterite slightly increases with lizardite addition. The presence of those new phases gave the sintered mixtures enhanced physico-chemical proper-

 DOI: https://doi.org/10.30564/jcr.v2i1.2684

ties with respect to the original raw materials.

Figure 9 showed the relative content of forsterite formation of M1-M4 series samples after firing at temperatures in the range of 1100–1400 °C for 2 h. The forsterite content exceeded 13.8 wt% in sample M4 after firing at 1100 °C, whereas the forsterite was absent in sample M1. After firing at 1400 °C, the relative content of the forsterite in sample M4 reached 42.7 wt% but remained at only 25.9 wt% in the sample M1. The relative content of forsterite in the sample M4 was greater than that in sample M1, M2 and M3 under the same firing temperature. This result indicates that finer lizardite powders contributed to a higher rate of forsterite formation. We conclude that the smaller lizardite particles enhanced the kinetics of the solid-state reactions and accelerated the rate of forsterite formation.

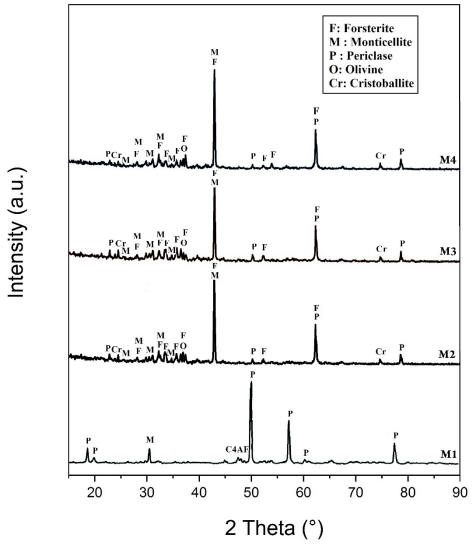

Figure 8. XRD patterns of the prepared mixtures at 1400 °C

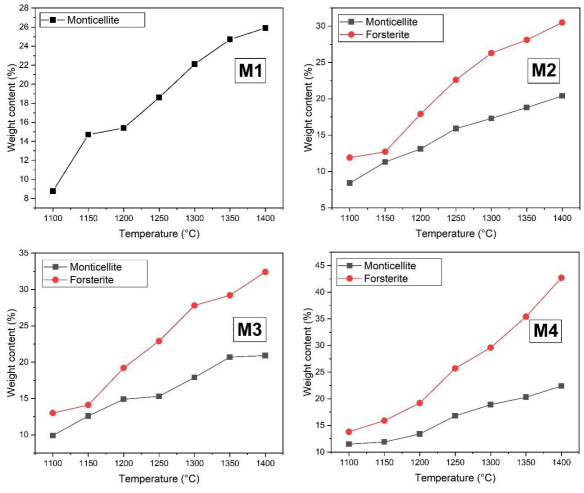

Figure 9. Relative content of forsterite and monticellite in M1-M4 mixtures after firing to the temperatures range of 1100–1400 °C for 2 h

Technological properties of fired mixtures were reported in Figure 10. An increased amount of lizardite in the initial mixtures stimulated the formation of more liquid phase upon calcination. The obtained results indicated that the prepared mixtures had increasing flexural strengths with augmented lizardite content. M4 sample recorded the highest flexural strength of 40.17 MPa. Data showed that firing shrinkage reached 8.52% for M1, but the addition of lizardite has led to a decrease in linear shrinkage during calcination up to 1400 °C. Low firing shrinkage values were observed for M2 (5.84%), M3 (3.7%), and M4 (2.9%).

The results of the Brazilian test varied between 19.34 MPa for M1 and 29.09 MPa for M4. Those value clearly satisfy the required technical specifications for ceramic industry. Such an increased consolidation may confirm the positive effects of lizardite addition via the activation of densification process which enhanced mechanical strength of the prepared ceramic mixtures. Figure 10.b shows the variation in bulk density and porosity as a versus lizardite contents of the prepared mixtures. It can be easily observed that M1 has the lowest bulk density (1.63 g/cm^3); that of M4 reached 3.25 g/cm^3. Similar results were obtained in previous studies [44-46]. In contrast, porosity decreased with bulk density. M1 yielded a porosity of 4.43% that decreased for M2, M3, M4, reaching 3.35, 1.9, and 0.89%, respectively. This can be attributed to the increase of the liquid phase with lizardite addition that directly affect the existing pore. Linear thermal expansion coefficients of all samples (i.e., M1, M2, M3 and M4) were ascertained of α_{M1}=1.7x10^{-5}/°C, α_{M2}=1.5x10^{-5}/°C, α_{M3}=1.25x10^{-5}/°C and α_{M4}=1.07x10^{-5}/°C). These results are in favor of good quality ceramics (Table 4).

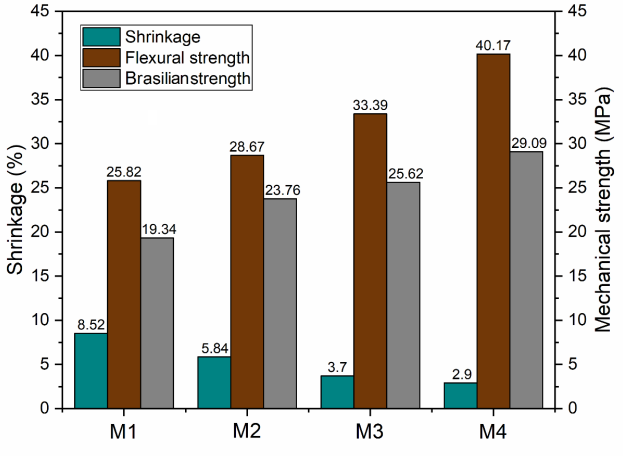

DOI: https://doi.org/10.30564/jcr.v2i1.2684

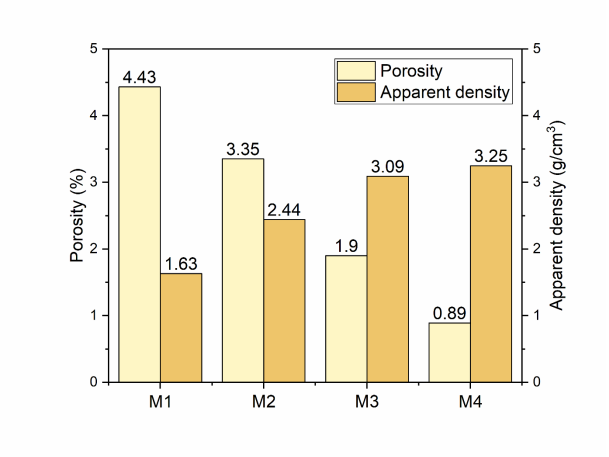

Figure 10. Technological properties of fired specimens at 1400 °C. a) Mechanical properties and b) Porosity and bulk density

Table 4. Thermal expansion coefficients of the fired specimens at 1400 °C/30 min

Samples	α_L (10^{-5}/°C)	α_V (10^{-5}/°C)
M1	1.70	5.10
M2	1.50	4.50
M3	1.25	3.75
M4	1.07	3.21

On the other hand, the tested samples have maintained their shape without undergoing any deformation up to 1400 °C (Figure. 11). They retain their original characteristics: no cracks, no deformation and low shrinkage at the end of the thermal cycle. The coloration is increasingly dark towards M4, which is due to the increase of iron oxides present in the started lizardite sample (6.68 %).

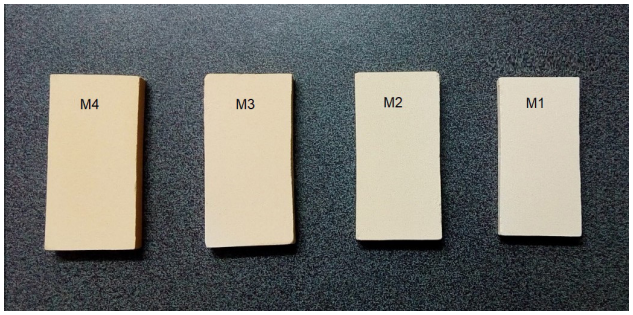

Figure 11. Aspect of samples fired at 1400 °C

The microstructure of the fired samples, having different content of lizardite were analysed using SEM. The micrographs shown in Figure 12 demonstrate significant effect of lizardite on the size and distribution of the particles on the surface. The surface morphologies of the samples are marked by the existence of particles with different grain sizes (1-10 µm) and distributions. The observation show that the formation of forsterite phase is highest in M4, supported by XRD analysis (Figure 9). Increase in grain size of forsterite, that is proportional to the amount of lizardite added, causes decrease in porosity (Figure 13), and subsequently, improving the mechanical properties ceramics (i.e., the flexural strength and Brazilian test).

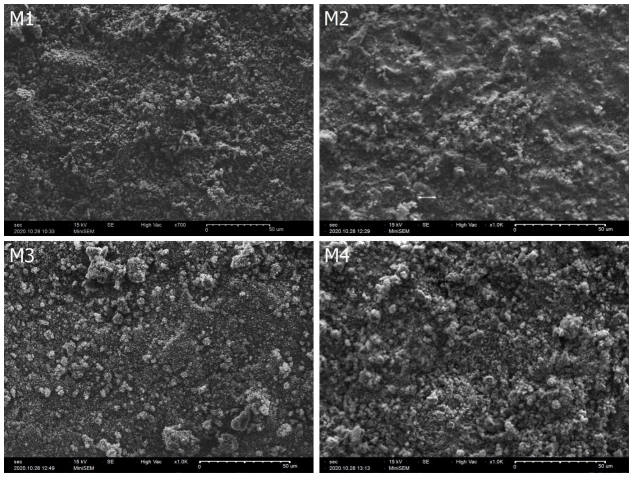

Figure 12. SEM micrographs of the mixtures fired at 1400 °C

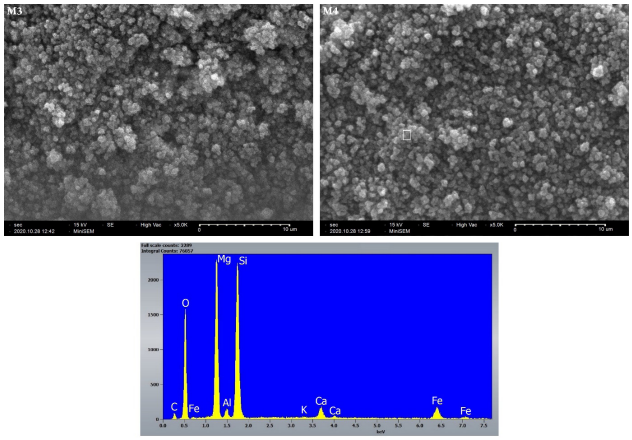

Figure 13. Microstructural analysis showing the porosity evolution by the SEM-EDS

4. Conclusions

This study has been carried out to evaluate the potential use of natural deposits from morocco for ceramic industry; the application concerned the Beni Bousra Massif (Rif domain, Southwestern Morocco) that showed important deposits of lizardite, magnesite and dolomite. Mineralogical analysis by X-ray diffraction on ceramic specimen from different mixtures confirmed the formation and co-

 DOI: https://doi.org/10.30564/jcr.v2i1.2684

existence of forsterite (Mg_2SiO_4) and monticellite ($CaMgSiO_4$). SEM observations showed increased densifications with temperature up to 1400 °C, proving that the addition of lizardite activated densification that contribute to the enhanced technological properties. An increased lizardite addition has led to a decrease in the linear shrinkage during calcination to 1400 °C.

Finally, the economic and social interest through the valorization of the numerous deposits will undoubtedly contribute to the sustainable development of this area. The preparation of lizardite-based ceramics was feasible with required technological properties, making from the Rif area a potential supplier of natural materials for ceramic industry.

CRediT authorship contribution statement

Ahmed Manni: Methodology, original draft, Laboratory operations.

Achraf Harrati: Methodology, original draft, Laboratory operations.

Abdelilah El Haddar: Sampling of raw material.

Abdelwahed Chari: Laboratory physico-chemical analysis (DRX and SEM).

Ali Sdiri: Writing manuscript and Revision.

Fahd Oudrhiri Hassani: Laboratory analysis (Thermodilatometric analysis), Reading manuscript and Revision.

Abdeslam El Bouari: Supervision and Validation.

Iz-Eddine El Amrani El Hassani: Study of the geological part and preparation of thin sections for observation under a microscope.

Chaouki Sadik: Scientific Direction, Results interpretation, Recommendations, Writing manuscript and Revision.

References

[1] C. Sadik, I. El Amrani, A. Albizane. Influence de la nature chimique et minéralogique des argiles et du processus de fabrication sur la qualité des carreaux céramiques. MATEC Web of Conferences, 2012, 2, Article ID: 01016.

[2] C. Sadik, I. Amrani, A. Albizane. Effect of carbon graphite on the crystallization of andalusite: Application to the synthesis of mullite and the improvement of refractory quality. Materials Sciences and Applications, 2013, 4(6): 337-346.

[3] C. Sadik, I. El Amrani, A. Albizane. Composition and ceramic characteristics of cretaceous clays from Morocco. Advances in Science and Technology, 2014, 92: 209-214.

[4] A. Harrati, A. Manni, A. El Bouari, I. El Amrani El Hassani, C. Sadik. Elaboration and thermomechanical characterization of ceramic-based on Moroccan geomaterials: Application in construction. Materials Today: Proceedings, 2020, 30: 876-882.

[5] C. Sadik, A. Manni, S. El Kalakhi, I. El Amrani, Preparation and characterization of possible basic ceramics from Moroccan magnesite. J Aust Ceram Soc, 2019, 55: 415-423.

[6] C. Sadik, I. El Amrani, A. Albizane. Processing and characterization of alumina-mullite ceramics. Journal of Asian Ceramic Societies, 2014, 2: 310-316.

[7] C. Sadik, I. Amrani, A. Albizane. Composition and refractory properties of mixtures of Moroccan silica-alumina geomaterials and alumina. New Journal of Glass and Ceramics, 2013: 59-66.

[8] A. Manni, B. Achiou, A. Karim, A. Harrati, C. Sadik, M. Ouammou, S. Alami Younssi, A. El Bouari. New low-cost ceramic microfiltration membrane made from natural magnesite for industrial wastewater treatment. Journal of Environmental Chemical Engineering, 2020, 8: 103906.

[9] C. Sadik, I. El Amrani, A. Albizane. Recent advances in silica-alumina refractory: A Review. Journal of Asian Ceramics Societies, 2014, 2: 83-96.

[10] A. Harrati, A. Manni, F.O. Hassani, A. Sdiri, S. El Kalakhi, A. El Bouari, I. El Amrani El Hassani, C. Sadik. Potentiality of new dark clay-rich materials for porous ceramic applications in Ouled Sidi Ali Ben Youssef Area (Coastal Meseta, Morocco). Journal of the Spanish Ceramic and Glass Society. In press.

[11] D.A. Brosnan, Alumina-silica brick, in: C.A. Schacht (Ed.), Refractories Handbook, Marcel Dekker Inc., New York, 2004: 79-107.

[12] C. Sadik, I. El Amrani, O. Moudden, A. El Bouari. Review on the elaboration and characterization of ceramics refractories based on magnesite and dolomite. Journal of Asian ceramics Societies, 2016, 4: 219-233.

[13] F. Wang, J. Ye, G. He, G. Liu, Z. Xie, J. Li. Preparation and characterization of porous MgAl2O4 spinel ceramic supports from bauxite and magnesite. Ceram. Int, 2015, 41: 7374-7380.

[14] Ghosh, C., Ghosh, A., Tripathi, H.S., Ghosh, J., Haldar, M.K. Studies on densification, mechanical, microstructural and structure–properties relationship of refractory aggregates prepared from Indian magnesite by changing lime–silica ratio. Ceram. Int, 2014, 40(16791-16798.

[15] Burhanuddin, A.,Kumar, P., Kumar, A.,Ghosh, S., Sinhamahapatra, S., Tripathi, H.S. Effect of zirconia on densification and properties of natural Indian

DOI: https://doi.org/10.30564/jcr.v2i1.2684

magnesite. Int. J. Miner. Process, 2015, 144: 40-45.
[16] Serry, M.A., El-Kholi, M.B., Elmaghraby, M.S., Telle, R. Characterization of Egyptian dolomitic magnesite deposits for the refractories industry. Ceram. Int, 2002, 28: 575-583.
[17] Rabah, M., Ewais, E.M.M. Multi-impregnating pitch-bonded Egyptian dolomite refractory brick for application in ladle furnaces. Ceram. Int, 2009, 35: 813-819.
[18] Ewais, E.M.M., Bayoumi, I.M.I., El-korashy, S.A. M-CZ composites from Egyptian magnesite as a clinker to RCK refractory lining. Ceram. Int, 2018, 44: 2274-2282.
[19] Saha, A., Singh, S.K., Ghosh, A., Ghosh, J., Haldar, M.K. Studies on synthesis and properties of magnesia refractory aggregates prepared from Indian magnesite through plasma fusion. Ceram. Int, 2015, 41: 2876-2883.
[20] Sinhamahapatra, S., Tripathi, H.S., Ghosh, A. Densification and properties of magnesia-rich magnesium-aluminate spinel derived from natural and synthetic raw materials. Ceram. Int, 2016, 42: 5148-5152
[21] Nan,W., Min, C., Yue-yuan, L., Hong-wei, N. Preparation of MgO whisker from magnesite tailings and its application. Trans. Nonferrous Metals Soc. China, 2011, 21: 2061-2065.
[22] Yuna, Z., Guocai, Z. A technology of preparing honeycomb-like structure MgO from low grade magnesite. Int. J. Miner. Process, 2014, 126: 35-40.
[23] Thomaidis, E., Kostakis, G. Synthesis of cordieriticmaterials using raw kaolin, bauxite, serpentinite/olivinite and magnesite. Ceram. Int, 2015, 41: 9701-9707.
[24] A. El Haddar, A. Manni, A. Azdimousa, I. El Amrani El Hassani, A. Bellil, C. Sadik, N. Fagel, M. El Ouahabi. Elaboration of a high mechanical performance refractory from halloysite and recycled alumina. Journal of the Spanish Ceramic and Glass Society, 2020, 59: 95-104.
[25] M. El Ouahabi, L. Daoudi, F.D. Vleeschouwer, R. Bindler, N. Fagel. Potentiality of Clay Raw Materials from Northern Morocco in Ceramic Industry: Tetouan and Meknes Areas, J. Min. Mat. Char. Eng, 2014, 2: 145-159.
[26] Kornprobst, J. Contribution à l'étude pétrographique et structurale de la zone interne du Rif, Notes et Mém. Serv. géol. Maroc, 1974, 251, 256.
[27] G.W. Brindley. Quantitative X-ray mineral analysis of clays. In: Brindley, G.W., Brown, G. (Eds.), Crystal Structures of Clay Minerals and Their X-ray Identification, Monograph 5. Mineralogical Society, London, 1980: 411-438.
[28] ASTM C674-88, Standard test methods for flexural properties of ceramic whiteware materials.
[29] R. H. Marion et K. Johnstone, A parametric study of the diametral compression test of ceramics, Am. Ceram. Soc. Bull, 1977, 56: 998.
[30] Fei Zhao, Lixin Zhang, Zhen Ren, Jinxing Gao, Xiaoyu Chen, Xinhong Liu, Tiezhu Ge. A novel and green preparation of porous forsterite ceramics with excellent thermal isolation properties. Ceramics International, 2019, 45: 2953-2961.
[31] ASTM C373-88, Standard test method for water absorption, bulk density, apparent porosity, and apparent specific gravity of fired whiteware products, Glass Ceramic, 2006: 15-02.
[32] J. B. Ferguson, H. E. Merwin. The Ternary System CaO-MgO-SiO2. Proceedings of the National Academy of Sciences of the United States of America, 1919, 5(1):16-18.
[33] M. Hajjaj, Mineralogy and thermal transformation of clay materials from the district of Marrakech, Morocco, Comunicações Geológicas, 2014, 101(1):75-80.
[34] Abi, C. E., Gürel, S. B., Kılınç, D., Emrullahoglu, Ö. F. Production of forsterite from serpentine–Effects of magnesium chloride hexahydrate addition. Advanced Powder Technology, 2015, 26(3): 947-953.
[35] Bain, D. C., Fraser, A. R. An unusually interlayered clay mineral from the eluvial horizon of a humus-iron podzol. Clay Minerals, 1994, 29:69-76.
[36] Manni, A., El Haddar, A., El Hassani, I. E. E. A., El Bouari, A., Sadik, C. Valorization of coffee waste with Moroccan clay to produce a porous red ceramics (class BIII). Boletín de la Sociedad Española de Cerámica y Vidrio, 2019.
[37] İ. Kıpçak, T.G. Isıyel, Magnesite tailing as low-cost adsorbent for the removal of copper (II) ions from aqueous solution, Korean J. Chem. Eng, 2015, 32: 1634-1641.
[38] M.B. Gawande, P.S. Branco, K. Parghi, J.J. Shrikhande, R.K. Pandey, C.A.A. Ghumman, N. Bundaleski, O.M.N.D. Teodoro, R.V. Jayaram, Synthesis and characterization of versatile MgO–ZrO2 mixed metal oxide nanoparticles and their applications, Catal. Sci. Technol, 2011, 1: 1653.
[39] Gopinath, D., Gunasekaran, S. The FTIR Spectra of Raw Magnesite and Sintered Magnesite, International Journal of Trend in Scientific, 2018, 2(4). ISSN No: 2456-6470.
[40] T.W. Cheng, Y.C. Ding, J.P. Chiu. A study of synthetic forsterite refractory materials using waste serpentine cutting. Minerals Engineering, 2002, 15: 271-275.

 DOI: https://doi.org/10.30564/jcr.v2i1.2684

[41] Hartman M, Trnka O, Vesely V, Svoboda K. Predicting the rate of thermal decomposition of dolomite. Chem Eng Sci, 1996, 51: 5229-32.

[42] Kristo´f-Mako E, Juha´sz AZ. The effect of mechanical treatment on the crystal structure and thermal decomposition of dolomite. Thermochim Acta, 1999, 342: 105-14.

[43] Fazeli AR, Tareen JAK. Thermal decomposition of rhombohedral double carbonates of dolomite type. J Therm Anal Calorim, 1991, 37, 2605-11.

[44] Zussman, J., R. Howie, W. Deer, An introduction to the rock forming minerals, Longman, UK, 1992.

[45] Soga, N., ANDERSON, O. L. High-temperature elasticity and expansivity of forsterite and steatite. Journal of the American Ceramic Society, 1967, 50(5): 239-242.

[46] Bafrooei, H. B., Ebadzadeh, T., Majidian, H. Microwave synthesis and sintering of forsterite nanopowder produced by high energy ball milling. Ceramics International, 2014, 40(2): 2869-2876.

DOI: https://doi.org/10.30564/jcr.v2i1.2684